Rotational bands in the semi-magic nucleus 5728Ni29

D Rudolph, I Ragnarsson, W Reviol, C Andreoiu, M A Bentley, M P Carpenter, R J Charity, R M Clark, M Cromaz, J Ekman, et al.

Rotational bands in the semi-magic nucleus $^{57}_{28}Ni_{29}$

D Rudolph[1], I Ragnarsson[2], W Reviol[3], C Andreoiu[1]‡, M A Bentley[4]§, M P Carpenter[5], R J Charity[3], R M Clark[6], M Cromaz[6], J Ekman[1]‖, C Fahlander[1], P Fallon[6], E Ideguchi[3]¶, A O Macchiavelli[6], M N Mineva[1] D G Sarantites[3], D Seweryniak[5] and S J Williams[4+]

[1] Department of Physics, Lund University, S-22100 Lund, Sweden
[2] Division of Mathematical Physics, LTH, Lund University, S-22100 Lund, Sweden
[3] Chemistry Department, Washington University, St. Louis, Missouri 63130, United States of America
[4] School of Chemistry and Physics, Keele University, Keele, Staffordshire, ST5 5BG, United Kingdom
[5] Physics Division, Argonne National Laboratory, Argonne, Illinois 60439, United States of America
[6] Nuclear Science Division, Lawrence Berkeley National Laboratory, Berkeley, California 94720, United States of America

E-mail: `Dirk.Rudolph@nuclear.lu.se`

Abstract. Two rotational bands have been identified and characterized in the proton-magic $N = Z + 1$ nucleus ^{57}Ni. These bands complete the systematics of well- and superdeformed rotational bands in the light nickel isotopes starting from doubly-magic ^{56}Ni to ^{60}Ni. High-spin states in ^{57}Ni have been produced in the fusion-evaporation reaction ^{28}Si(^{32}S,$2p1n$)^{57}Ni and studied with the γ-ray detection array GAMMASPHERE operated in conjunction with detectors for evaporated light charged particles and neutrons. The features of the rotational bands in ^{57}Ni are compared to those of neighbouring isotopes and interpreted by means of configuration-dependent cranked Nilsson-Strutinsky calculations. The two observed high-spin bands are considered signature partners and assigned to configurations with one $1g_{9/2}$ proton and one $1g_{9/2}$ neutron, resulting in an unambiguous understanding of the energetically favoured signature $\alpha = -1/2$ band but a somewhat less satisfactory description of the signature $\alpha = +1/2$ band.

PACS numbers: 21.60.Cs, 23.20.En, 23.20.Lv, 27.40.+z

Submitted to: *J. Phys. G: Nucl. Phys.*

‡ Present address: Chemistry Department, Simon Fraser University, Burnaby, BC, V5A 1S6, Canada
§ Present address: Department of Physics, University of York, York, YO10 5DD, United Kingdom
‖ Present address: Malmö högskola, S-20506 Malmö, Sweden
¶ Present address: Center for Nuclear Study, University of Tokyo, Saitama 351-0198, Japan
+ Present address: TRIUMF, Vancouver, BC, V6T 2A3, Canada

1. Introduction

Spectroscopic observables of doubly-magic nuclei and isotopes in their close vicinity represent benchmarks of effective nucleon-nucleon interactions, which remain key ingredients of any contemporary nuclear model. In particular medium-mass nuclei are interesting in that respect, since they are accessible by different microscopic and macroscopic-microscopic theoretical treatments. As prime examples, the doubly-magic and hence near-spherical $N = Z = 20$ and $N = Z = 28$ nuclei ^{40}Ca and ^{56}Ni have revealed coexisting strongly deformed rotational spectra already at modest excitation energies and angular momenta [1, 2]. For instance, extensive large-scale shell-model calculations [2, 3, 4], Monte-Carlo shell-model calculations [5], complex variational calculations [6], or cranked Hartree-Fock and Hartree-Fock-Bogolyubov calculations [2] as well as the cranked Nilsson-Strutinsky approach [7] have been applied to characterize and describe shape coexistence in ^{56}Ni.

In addition, neutron-deficient $N \sim Z$ nuclei in the mass $A \sim 60$ regime have been established as a region of well- and superdeformed (SD) nuclear shapes. The region is centered around the $N = Z = 30$ 'doubly-magic superdeformed' core ^{60}Zn [8], owing to a significant prolate shell gap at particle number 30, which holds for a wide range of high angular momentum [9]. This gap, which is related to the particle number 28 shell gap at the 2:1 axis ratio ($\varepsilon_2 = 0.6$) of the harmonic oscillator [10], is characterized by having four particles in $\mathcal{N} = 4$, $1g_{9/2}$ intruder orbitals and four holes in the $\mathcal{N} = 3$, $1f_{7/2}$ extruder orbitals, which are all strongly shape driving. With this background, bands in this mass region which are built on a similar number of particle-hole excitations are generally referred to as superdeformed even though their deformations are often much smaller than $\varepsilon_2 = 0.6$ [8, 11, 12].

At intermediate spins and excitation energies, these SD bands often compete with less deformed bands, which contain a smaller number of cross-shell excitations in their configuration. In fact, the average amount of quadrupole deformation of a specific rotational $A \sim 60$ band has been found to essentially scale with the sum of number of holes in the $1f_{7/2}$ orbital and number of particles in the $1g_{9/2}$ orbital [13]. Subsequently and somewhat different from these energetically favoured cases at or near $N = Z$, a plethora of rotational bands has been found in a number of $N > Z$ nuclei, which often are less straight-forward to characterize, namely in $^{57}_{27}$Co [14], $^{58-60}$Ni [15, 16, 17, 18, 19], ^{61}Cu [21, 22], or ^{61,62}Zn [21, 22, 23, 24].

One missing link is the presence of deformed structures in ^{57}Ni, which due to its $N = Z + 1$ nature is expected to provide only a limited number of energetically favored rotational bands; these are reported and discussed here, thus closing the nickel chain from ^{56}Ni to ^{60}Ni. Near-spherical medium-spin states of ^{57}Ni have been studied in detail in [25, 26, 27]. Indeed, these studies form a proper basis for the present extension towards rotational high-spin states. Preliminary results on such a rotational band in ^{57}Ni have been presented in [28]. Section 2 provides information on the experimental approach and the data analysis, and the experimental results are the subject of Section 3.

The bands in ^{57}Ni are discussed and characterized by means of configuration-dependent Nilsson-Strutinsky calculations in Section 4.

2. Experiments and Data Analysis

The present study relies on data from two almost identical experiments. Details are given in [29, 30, 31]. A ^{32}S heavy-ion beam impinged with an energy of 130 MeV on isotopically enriched 0.5 mg/cm^2 ^{28}Si targets inducing fusion-evaporation reactions. The targets were supported with $\sim$1 mg/cm^2 Ta or Au foils. These faced the beam and thus led to an effective mid-target beam energy of about 122 MeV. The γ-rays were detected in the GAMMASPHERE germanium-detector array [32], which comprised 78 Ge-detectors with associated anti-Compton suppression shields. The Heavimet collimators in front of these suppression shields were removed to allow for event-by-event γ-ray calometric and fold information. This can provide additional reaction channel selectivity by so-called total-energy gating [33]. Both experiments employed the 4π CsI-array MICROBALL [34], which is used to detect evaporated light charged particles. The NEUTRON SHELL [35] replaced about one third of GAMMASPHERE in forward direction to allow for the detection of evaporated neutrons.

The details of the data handling and data analysis of the two experiments have also been described earlier [29, 30, 31]. In brief, standard pulse-shape discrimination techniques are used to distinguish different light charged particles in MICROBALL, mainly protons and α-particles [34, 36], and to discriminate neutrons from γ-rays detected in the liquid-scintillator detectors of the NEUTRON SHELL [35, 37].

Since the directions and energies of the evaporated particles are known, an event-by-event kinematic reconstruction can be performed, which leads to a much improved Doppler correction of the emitted γ-rays, provided they are emitted after the recoiling nucleus left the thin target foil. This is *not* the case for most of the γ-ray transitions originating from well- or superdeformed bands, i.e. the lifetimes of the associated rotational states do not exceed the transit time of the recoils through the target ($\leq$ 200 fs). Therefore, the corresponding peaks in the γ-ray spectra become broader than γ-ray peaks from normally deformed (ND) and usually longer-lived states. However, this additional Doppler shift for fast transitions can be accounted for by assuming an average deformation, hence quadrupole moment, of the rotational bands, which in conjunction with the modelling of the slowing-down process in the thin target foil yields revised higher velocities of the recoils at the time of γ-ray emission. The use of such a scheme sharpens the peaks belonging to rotational bands in the γ-ray spectra, while in turn peaks belonging to ND states become broader. In fact, investigating spectra with and without the additional correction provides useful hints on whether or not a γ-ray transition belongs to a SD band, its decay-out regime, or the lower-lying ND section of the excitation scheme. For the present study, all spectra and $\gamma\gamma$ correlation matrices and $\gamma\gamma\gamma$ correlation cubes use the refined Doppler correction. In the work of Reviol *et al* [28], an average quadrupole moment for one of the bands in ^{57}Ni has been derived

by investigating these additional Doppler shift effects in some more detail. While the suggested value of $Q_0 = 2.3^{+0.9}_{-0.7}$ eb clearly hints towards a very large deformation of the rotational structure, the limited statistics prevented (and prevents) to deduce a more precise value, which would be necessary to distinct between different theoretical descriptions.

Judging from the yields of prominent γ-ray transitions of all residual nuclei observed in the ^{32}S+^{28}Si reaction and taking into account the detection efficiencies of $\epsilon_p = 65(1)\%$ for protons, $\epsilon_\alpha = 50(2)\%$ for α particles, and $\epsilon_n = 25(1)\%$ for neutrons for the present experiments, the $2p1n$ reaction channel leading to ^{57}Ni is found to account for less than 2% of the total fusion-evaporation cross-section. Therefore, the detection of exactly two evaporated protons and in particular one evaporated neutron is needed to discriminate γ-ray transitions associated with ^{57}Ni residues against the overwhelming 'background' of γ rays originating from more abundant reaction channels, even though the statistics in the γ-ray objects used in the ^{57}Ni analysis is reduced by about an order of magnitude.

Major remaining contaminations in the analysis originate from the $3p1n$ channel ^{56}Co [38], which leaks into the $2p1n$ γ-ray object in case one proton missed detection. A considerable fraction of such contaminants can be suppressed by applying the selection method described in [33], and by eventually subtracting spectra with an additional, third proton required in coincidence. The Radware software package [39] and the tailored γ-ray spectroscopy analysis code Tv [40], which has been developed at the University of Cologne, were used to construct the level scheme and derive the relative intensities of the γ-ray transitions.

Due to limited statistics, multipolarity assignments of transitions are based on ratios of yields R_{150-97} [26]. This is the ratio of efficiency-corrected γ-ray yields measured in the three most backward oriented rings of Gammasphere (average angle $\overline{\theta} = 150^\circ$ with respect to the beam axis) versus the corresponding yield for the central section of Gammasphere ($\overline{\theta} = 97^\circ$) (cf. [26]). To ensure selectivity, coincidences are required with relevant γ-ray transitions from ^{57}Ni detected anywhere in the Ge-detector array ($\overline{\theta} = 124^\circ$). Stretched quadrupole transitions should reveal $R_{150-97} \sim 1.2$-1.3, whereas stretched dipole transitions are predicted to have $R_{150-97} \sim 0.8$. Smaller or larger values are indicative for mixed $\Delta I = 1$, $E2/M1$ transitions. Pure non-stretched ($\Delta I = 0$) dipole transitions have values similar to quadrupole transitions.

3. Experimental Results

The results of the data analysis are illustrated in figure 1 and summarized in table 1. Figure 1 provides the relevant part of the decay scheme of ^{57}Ni, focusing on the two new high-spin rotational sequences SD1 and SD2 on the left-hand side and their decay-out. Compared with [25, 26, 27], the $I^\pi = (25/2^-)$ level at 10974 keV excitation energy has been added, and some spin-parity assignments have been possible in the band-like structure B1 in the centre of the figure (cf. table 1).

The spectrum in panel (c) of figure 2 selects exclusively γ-ray transitions belonging

to ^{57}Ni. It is taken in coincidence with either the 1287 or 2577 keV transition of the $11/2^- \rightarrow 7/2^- \rightarrow 3/2^-$ ground-state cascade of ^{57}Ni and the reaction channel selection described in Section 2. Next to the transitions known to belong to ^{57}Ni, this spectrum reveals rather intense peaks at, for instance, 1694, 2087, 2120, $\sim$ 2505, and $\sim$ 2965 keV. These peaks dominate the spectrum in figure 2(c) beyond $E_\gamma = 2$ MeV – besides the 2577 keV ground-state transition. They are found to form two rather intense rotational bands at high spin in ^{57}Ni, SD1 and SD2.

The spectra in the lower part of figure 2 document the analysis of SD2. Panel (d) shows transitions in coincidence with the band members at 1746, 2120, 2500, 2959, and 3239 keV. (Note that the 1746 keV transition of SD2 is a doublet with the 1745 keV transition in structure B1.) Next to the members of SD2, including the lower-lying 1386 keV transition, the spectrum in figure 2(d) reveals peaks from decays of all relevant ND states, in particular at 968 and 1818 keV (B1), and the related peak at 3349 keV. The former peaks are members of the B1 structure, namely the decays from the 9856 keV, $23/2^-$ state. The latter peak connects the 13205 keV state of SD2 with just that ND level. This is proven in figure 2(e), which shows the γ-ray spectrum in coincidence with the 3349 keV link. The transitions in SD2 are seen with decreasing yield (starting at 1746 keV), the 968 and 1818 keV are pronounced, and the flux is collected again in the 1287, 1455, and 2577 keV members of the ground-state sequence. The angular distribution ratio of the 3349 keV line, $R_{150-97} = 0.90(12)$, indicates (pure) dipole character. This affirms a spin assignment $I = 25/2$ for the state at 13205 keV. However, the parity of SD2 cannot be determined experimentally since the data is unable to distinguish between $M1$ or $E1$ character of the 3349-keV linking transition. The angular distribution ratios of the members on top of the 13205 keV level are all consistent with stretched quadrupole character, establishing the band up to the 25769 keV, $I = 45/2$ state. Between 15 and 20 MeV excitation energy, SD2 carries about 10 % of the yield of the 2577 keV ground-state transition.

Panels (a) and (b) of figure 2 focus on SD1. Panel (b) is created in a similar fashion as panel (d); it is the sum of spectra in coincidence with the band members at 1694, 2087, 2508, 2973, and 3377 keV. Though close in energy, the SD1/SD2 doublets at 2973/2959 and 2508/2500 can be resolved in the coincidence analysis. This is indicated by the vertical dashed lines in figure 2. In addition to the band members mentioned, transitions at 1306, 1614, 3610, 3696, and 4308 keV are enhanced. With an angular distribution ratio of $R_{150-97} = 1.32(15)$, the 1306 keV line most likely continues SD1 to lower spin values. The 1614-keV line, however, is found to be a dipole transition. The subsequent decay pattern following the 1614-keV transition could not be delineated, while its relative yield in combination with the lack of coincidences with, for example, the lines at 1306 and 4308-keV ensure the placement in figure 1.

The three high-energy lines are clearly visible in the insets of panels (b) and (c). While the transitions at 3610 and 4308 link SD1 with the ND states, the peak at 3696 keV is most likely associated with SD1 but could not be placed unambiguously in the decay scheme of figure 1. Figure 2(a) represents the spectrum in coincidence

with the 4308 keV line. It is found to feed the 9495 keV $23/2^-$ yrast state, since the spectrum shows peaks at 890, 906, 1151, 1924, 1939, and 2042 keV next to the SD1 band members and the 1455-1287-2577 keV ground-state sequence. Furthermore, the 3610 keV line fits the energy gap between the lowest state of SD1 at 12497 keV and the 8888 keV $21/2^-$ level in B1 and concurs with the necessary coincidence relationships. The angular distribution ratios of the 3610 and 4308 keV lines provide values consistent with $\Delta I = 1$, mixed $E2/M1$ and $E2$ character, respectively, which in combination allows for a firm spin and parity assignment of SD1. Finally, SD1 comprises a yield of about 25 % of the 2577 keV transition in the excitation energy range of 15 to 20 MeV. This is a remarkably large number similar to, for example, the favoured deformed band in the neighbouring isotope ^{58}Cu [12]. The higher yield of SD1 over SD2 is also a clear sign for SD1 lying closer to (or likewise marking) the yrast line at very high spin in ^{57}Ni. This is consistent with the spin assignments of both bands based on the angular distribution ratios of the linking transitions and the absence of any other hitherto unknown intense peaks in the ^{57}Ni reference spectrum in figure 2(c). Finally, transitions connecting SD1 and SD2 have not been observed in the present data.

Another note concerns the possibility of prompt, discrete-energy particle decays, which are known in the $A \sim 60$ region to connect rotational states in the decay-out regime with near spherical states in the respective daughter nuclei [7, 12, 15, 17]. Taking $S_p = 7332$ keV [41] and assuming a $1g_{9/2}$, $\ell = 4$ proton decay of the 13205 keV level in SD2, the yrast 8^+ state at 3638 keV in ^{56}Co [38] could be reached with $Q_p = 13205 - (7332 + 3638)$ keV $= 2235$ keV, a value similar to existing cases. A similar option can be estimated for the 11819 keV state at the bottom of SD2, while the lack of rather low-lying negative-parity states with matching spins in ^{56}Co prohibit a solid estimate for proton decay energies from states in SD1. Nevertheless, a search for proton decays from both SD1 and SD2 into low-lying excited states of ^{56}Co has been performed but proved negative. The phase space for α decay of low-lying states of SD1 and SD2 is considered too low compared with the known cases in ^{58}Ni [15, 17].

4. Discussion

The observed SD bands of ^{57}Ni are interpreted from comparisons with the bands calculated in the configuration dependent cranked Nilsson-Strutinsky (CNS) model [9, 42, 43]. This model is based on a modified oscillator potential which is cranked around the x-axis. The total energy of the different bands is obtained from the sum of the single-particle energies of the orbitals, which are occupied in a specific configuration. This sum is calculated at the value of the rotational frequency, which corresponds to a specific spin value obtained from the sum of the expectation values of the j_x operator. The configurations are defined by the filling of the different groups of orbitals, which are specified by the $\mathcal{N}$-shells — or rather $\mathcal{N}_{rot}$-shells — and the signature quantum number, α. When possible, i.e. generally at small deformation, a distinction is also made between orbitals of high-j and low-j character, respectively.

The energies of the different configurations are Strutinsky renormalized [44] to a rotating liquid-drop energy based on the Lublin-Strasbourg drop model (LSD) [45]. Rigid moments of inertia are calculated from a nucleus with a diffuse surface having a radius parameter $r_0 = 1.16$ fm and a diffuseness parameter, $a = 0.6$ fm [43]. The total energies are then generally shown relative to the rotating liquid drop energy, based on the same LSD model and minimized with respect to deformation at each spin value.

In the CNS calculations the standard modified oscillator single-particle parameters are used [42] but with an increased gap at proton number $Z = 28$. This modification was introduced in [16] such that the crossing frequency between the bands with two and three $1f_{7/2}$ proton holes comes at the observed spin value in ^{58}Ni. This is achieved by increasing the distance between the high-j ($1f_{7/2}$) and low-j ($2p_{3/2}$, $1f_{5/2}$, and $2p_{1/2}$) subshells by 0.0423 $\hbar\omega_0$ corresponding to ~ 0.4 MeV, while keeping their centre of mass unchanged. In a similar way as for ^{58}Ni, the modification of the single-particle energies has only a minor influence on the calculated bands, but it moves the crossing between the bands with two and three $1f_{7/2}$ proton holes to somewhat higher spin values ($\Delta I \sim 2\hbar$).

It is instructive to first compare the SD bands in ^{57}Ni with similar bands in the neighbouring Ni isotopes as presented in figure 3. A representation is chosen where the energies are plotted relative to the rotating liquid drop. The figure suggests a continuous trend from SD2 in ^{56}Ni via SD1 in ^{57}Ni to the SD bands in ^{58}Ni. The bands in ^{56}Ni and ^{58}Ni are labelled according to previous interpretations by the number of $1f_{7/2}$ holes, p_1 and n_1, and $1g_{9/2}$ particles, p_2 and n_2, respectively, for protons and neutrons, $[p_1p_2, n_1n_2]$. It can be seen in figure 3 that in the low-spin range of the respective bands, the two additional neutrons in ^{58}Ni compared with ^{56}Ni are placed in the $1g_{9/2}$ shell. This suggests that the yrast SD1 band in ^{57}Ni simply lies in between, i.e. it has one additional $1g_{9/2}$ neutron relative to the band SD2 in ^{56}Ni.

The observed bands SD1 and SD2 of ^{57}Ni are redrawn in the upper panel of figure 4. They are compared with the calculated bands having one $1g_{9/2}$ proton and one $1g_{9/2}$ neutron shown in the middle panel of figure 4, relative to the same reference rotating liquid drop energy, E_{rld}. The two lowest bands of each signature are calculated with no attempt to distinguish between high-j and low-j orbitals. However, when comparing with the single-particle orbitals shown in figure 5, it becomes possible to determine the configurations of the calculated bands in more detail. Figure 5 is drawn for protons but due to its $N \sim Z$ nature, the neutron orbitals of ^{57}Ni behave very similar. In fact, the rather stable neutron configuration is based on the large gap associated with 29 particles, which dominates the approximate frequency range of 0.5–2.0 MeV in figure 5 and which is responsible for the exclusive $[21, 21]$ band known in ^{58}Cu ($N = Z = 29$) [12]. This configuration implies that the highest $1f_{7/2}$ orbital, which can be seen to be signature degenerate up to $\hbar\omega = 2.0$ MeV, is empty, i.e. the most stable neutron configuration for low-lying rotational bands in ^{57}Ni is also $, n_1n_2] =, 21]$. The calculated deformation for these configurations — $\varepsilon_2 \sim 0.32$ at spin $I \sim 21\ \hbar$ — is not very large. This can be understood from the fact that while there are four or five holes in the $1f_{7/2}$ orbitals defining the underlying SD gap, there are only two particles in $1g_{9/2}$ orbitals.

Nevertheless, the deformation is consistent with the average quadrupole deformation reported in [28].

For the 28 protons of ^{57}Ni and with one of them in the lowest $1g_{9/2}$ orbital, there is the necessity for one proton hole in the orbitals of either $2p_{3/2}1f_{5/2}$ — labelled (fp) in figure 5 — or $1f_{7/2}$ character below the $Z = 29$ gap. At low frequencies, the lowest energy band will have a hole in the (fp) orbitals corresponding to a $[p_1p_2, =$ [21, configuration. Then, however, the $1f_{7/2}$ and (fp) orbitals come close in energy and exchange character at $\hbar\omega \approx 1.5$ MeV. Consequently, at higher frequencies the lowest energy band is expected to have the hole in an orbital of $1f_{7/2}$ character instead, which thus corresponds to a $[p_1p_2 =$ [31, configuration. One could also note that two bands with a hole in the signature degenerate $1f_{7/2}$ orbital would be expected to be connected by $M1$ transitions at low frequencies. The absence of such transitions in ^{57}Ni supports the present interpretation that the SD1 and SD2 bands have a hole the (fp) orbital in the low-spin range.

The comparison between calculations and experiment in figure 4 shows that the SD1 band is very well described by the calculated lowest energy band with one $1g_{9/2}$ proton and one $1g_{9/2}$ neutron; the difference curve in the lower panel is almost horizontal, which means that the transition energies are nicely reproduced. The absolute value of the difference is off by approximately -1 MeV, i.e. it has a value which is within the range of the typically expected accuracy, ± 1 MeV. The straightforward conclusion is that the SD1 band should be associated with the $[21, 21]$ configuration and that it gradually changes its configuration towards $[31, 21]$ at $\hbar\omega \approx 1.5$ MeV, i.e. close to the highest spin values observed. This configuration change receives support from the differences in the transition energies, ΔE_γ. Starting from the 23/2 state at the bottom of the band, the values are $\Delta E_\gamma = 388$, 393, 421, 465, and 404 keV, i.e. this difference suddenly decreases at the top. This corresponds to an increasing $\mathcal{J}^{(2)}$ moment of inertia and hence suggests that the highest spin state is pushed down from an interaction with another band. Such a crossing between the $[21, 21]$ and $[31, 21]$ configurations is also consistent with the general trends seen in figure 3 and discussed in [16].

The SD2 band is somewhat more difficult to describe theoretically. The parity is not determined, and therefore both positive- or negative-parity bands have to be considered. To generate energetically competitive positive-parity bands, configurations with either one or three $1g_{9/2}$ particles need to be considered. Therefore, the lowest calculated band with one $1g_{9/2}$ particle, namely $[20, 21]$, is included in figure 4. It is evident that this band has a very different behaviour than both the observed SD1 and SD2 bands with a strong increase relative to the reference in the spin range $I = 10 - 20$. Interestingly, however, the 12189 keV, $I = 25/2$ level could be interpreted as a member of this $[20, 21]$ band. The 1614-keV transtion would then mark an $E1$ link between the $[21, 21]$ and the $[20, 21]$ bands in ^{57}Ni in close resemblance to the 1626-keV ($E1$) link connecting the corresponding $[21, 20]$ and $[20, 20]$ bands in ^{56}Ni [2, 7].

Similarly, positive-parity bands having three $1g_{9/2}$ particles show a strong decrease relative to the reference in the spin range $I = 20 - 30$, which once more is very different

from the trend of both bands observed in ^{57}Ni. It is thus safe to interpret also the SD2 band in ^{57}Ni as a negative-parity band with two $1g_{9/2}$ particles, i.e. it relates to the bands of this type shown in the middle panel of figure 4 as well, but with the opposite signature compared with SD1. Using an assignment to the lowest band with signature $\alpha = +1/2$, the difference comes out as drawn by the dashed line and filled circles in the corresponding lower panel. It is, however, evident that the calculated band, which should be labelled $[21, 21]$ at low spin, interacts with and comes close to the $[31, 21]$ band at $I = 41/2$. Assuming that these two bands cross, the two crossing bands will appear as drawn by dotted lines. The two crossing bands would then be labelled $[21, 21]$ and $[31, 21]$ over the full spin range. If SD2 were assigned to this $[21, 21]$ band, the difference comes out as shown by a dotted line in the lower panel of figure 4. This difference is clearly an improvement compared with the one based on the original band assignment indicated by the dashed line. However, the slope of the difference curve remains unsatisfactorally large.

5. Summary

In conclusion, two SD bands have been observed in the $N = Z + 1$ nucleus ^{57}Ni in the reaction ^{28}Si($^{32}S, 2pn$) by means of prompt particle-$\gamma\gamma$ and -$\gamma\gamma\gamma$ coincidence investigations using the Gammasphere Ge-detector array in conjunction with the Microball and Neutron Shell ancillary devices. Based on cranked Nilsson-Strutinsky calculations the two bands are interpreted as signature partners having the CNS configuration $[21, 21]$ in the spin range $I = 10$–20. Around spin $I = 20$, however, the predicted $[21, 21]$ bands are expected to interact with $[31, 21]$ bands, and in particular the signature $\alpha = +1/2$ branch. For a complete and thorough understanding it would therefore be of great value if the respective non-yrast sections of the two $[21, 21]$ and the two $[31, 21]$ negative-parity bands could be discriminated experimentally. This is, however, difficult with present-day instrumentation and beam-target combinations. Nevertheless, the unambigous experimental characterisation and theoretical assignment of the yrast SD band in ^{57}Ni provides an important link in the nickel chain for a complete assessment of superdeformation in the $A \sim 60$ region.

Acknowledgments

First of all, we would like to thank the accelerator crews and the Gammasphere support staff at Argonne and Berkeley for their supreme efforts. The target maker, Jette Agnete Sørensen, at the Niels Bohr Institute, Copenhagen, Denmark, is also warmly thanked. This work is supported in part by the Swedish Research Council and the U.S. Department of Energy under grants No. DE-AC03-76SF00098 (LBNL), DE-FG05-88ER-40406 (WU), and W-31-109-ENG38 (ANL).

References

[1] Ideguchi E *et al* 2001 *Phys. Rev. Lett.* **87** 222501
[2] Rudolph D *et al* 1999 *Phys. Rev. Lett.* **82** 3763
[3] Horoi M, Brown B A and Zelevinsky V 2003 *Phys. Rev. C* **67** 034303
[4] Horoi M, Brown B A, Otsuka T, Honma M and Mizusaki T 2006 *Phys. Rev. C* **73** 061305(R)
[5] Mizusaki T, Otsuka T, Honma M and Brown B A 2001 *Phys. Rev. C* **63** 044306
[6] Petrovici A, Schmid K W and Faessler A 2001 *Nucl. Phys. A* **689** 707
[7] Johansson E K *et al* 2008 *Phys. Rev. C* **77** 064316
[8] Svensson C E *et al* 1999 *Phys. Rev. Lett.* **82** 3400
[9] Afanasjev A V, Ragnarsson I and Ring P 1999 *Phys. Rev. C* **59** 3166
[10] Ragnarsson I, Nilsson S G and Sheline R K, *Phys. Rep.* **45** 1
[11] Andreoiu C *et al* 2000 *Phys. Rev. C* **62** 051301(R)
[12] Rudolph D *et al* 1998 *Phys. Rev. Lett.* **80** 3018
[13] Andreoiu C *et al* 2002 *Eur. Phys. J.* **A14** 317
[14] Reviol W *et al* 2002 *Phys. Rev. C* **65** 034309
[15] Rudolph D, Baktash C, Devlin M, LaFosse D R, Riedinger L L, Sarantites D G and Yu C-H 2001 *Phys. Rev. Lett.* **86** 1450
[16] Rudolph D *et al* 2006 *Phys. Rev. Lett.* **96** 092501
[17] Johansson E K *et al* 2009 *Phys. Rev. C* **80** 014321
[18] Yu C-H *et al* 2002 *Phys. Rev. C* **65** 061302(R)
[19] Torres D A *et al* 2008 *Phys. Rev. C* **78** 054318
[20] Andersson L-L *et al* 2008 *Eur. Phys. J.* **A36** 251
[21] Yu C-H *et al* 1999 *Phys. Rev. C* **60** 031305(R)
[22] Andersson L-L *et al* 2009 *Phys. Rev. C* **79** 024312
[23] Svensson C E *et al* 1998 *Phys. Rev. Lett.* **80** 2558
[24] Gellanki J *et al* 2009 *Phys. Rev. C* **80** 051304(R)
[25] Spohr K *et al* 1995 *Acta Phys. Pol.* **B26** 297
[26] Rudolph D, Baktash C, Brinkman M J, Devlin M, Jin H-Q, LaFosse D R, Riedinger L L, Sarantites D G and Yu C-H 1999 *Eur. Phys. J.* **A4** 115
[27] Rudolph D, Weisshaar D, Cristancho F, Eberth J, Fahlander C, Iordanov O, Skoda S, Teich Ch, Thelen O and Thomas H G 1999 *Eur. Phys. J.* **A6** 377
[28] Reviol W *et al* 2001 *Nucl. Phys. A* **682** 28c
[29] Ekman J *et al* 2002 *Phys. Rev. C* **66** 051301(R)
[30] Ekman J *et al* 2004 *Phys. Rev. C* **70** 014306
[31] du Rietz R *et al* 2005 *Phys. Rev. C* **72** 014307
[32] Lee I-Y 1990 *Nucl. Phys. A* **520** 641c
[33] Svensson C E *et al* 1997 *Nucl. Instr. Meth. A* **396** 288
[34] Sarantites D G *et al* 1996 *Nucl. Instr. Meth. A* **381** 418
[35] Sarantites D G *et al* 2004 *Nucl. Instr. Meth. A* **530** 473
[36] Andreoiu C 2002, PhD thesis, Lund University, ISBN 91-628-5308-2
[37] Ekman J 2004, PhD thesis, Lund University, ISBN-91-628-6061-5
[38] Palacz M *et al* 1997 *Nucl. Phys. A* **627** 162
[39] Radford D C 1995 *Nucl. Instr. Meth. A* **386** 297
[40] Theuerkauf J, Esser S, Krink S, Luig M, Nicolay N, Stuch O and Wolters H, program TV, University of Cologne, unpublished.
[41] Audi G, Wapstra A H and Thibault C 2003 *Nucl. Phys. A* **729** 337
[42] Bengtsson T and Ragnarsson I 1985 *Nucl. Phys. A* **436** 14
[43] Carlsson B G and Ragnarsson I 2006 *Phys. Rev. C* **74** 011302(R)
[44] Strutinsky V M 1967 *Nucl. Phys. A* **95** 420
[45] Pomorski K and Dudek J 2003 *Phys. Rev. C* **67**, 044316

Table 1. Level energies, E_x, γ-ray energies, E_γ, γ-ray intensities relative to the 2577 keV ground-state transition in ^{57}Ni, Y_γ, angular-distribution ratios, R_{150-97}, and multipolarities, as well as spin-parity assignments of initial and final states, I_i^π and I_f^π. Parentheses indicate tentative assignments.

E_x (keV)	E_γ (keV)	Y_γ (%)	R_{150-97}	multi-polarity	I_i^π ($\hbar$)	I_f^π ($\hbar$)
B1						
7142(1)	723(1)	3(1)	—	$\Delta I = 0$	$17/2^-$	$17/2^-$
	1630(1)	3(1)	0.99(10)	$E2/M1$	$17/2^-$	$15/2^-$
8038(1)	585(1)	2(1)	—	$\Delta I = 0$	$19/2^-$	$19/2^-$
	896(1)	2(1)	—	$E2/M1$	$19/2^-$	$17/2^-$
	1620(1)	4(1)	0.72(15)	$E2/M1$	$19/2^-$	$17/2^-$
	2526(2)	2(1)	—	$E2$	$19/2^-$	$15/2^-$
8888(1)	545(1)	1(1)	—	$\Delta I = 0$	$21/2^-$	$21/2^-$
	1745(2)	5(1)	1.27(9)[a]	$E2$	$21/2^-$	$17/2^-$
9856(1)	968(1)	2(1)	1.05(19)	$E2/M1$	$23/2^-$	$21/2^-$
	1818(2)	3(1)	1.55(20)	$E2$	$23/2^-$	$19/2^-$
10974(1)	1119(2)	2(1)	—	$(E2/M1)$	$(25/2^-)$	$23/2^-$
	2084(2)	3(1)	1.25(7)[a]	$(E2)$	$(25/2^-)$	$21/2^-$
SD1						
12497(2)	3610(3)	2(1)	0.48(11)	$E2/M1$	$23/2^-$	$21/2^-$
13803(2)	1306(1)	3(1)	1.32(15)	$E2$	$27/2^-$	$23/2^-$
	1614(2)	4(1)	0.83(10)	$\Delta I = 1$	$27/2^-$	25/2
	3946(4)	1(1)	—	$E2$	$27/2^-$	$23/2^-$
	4308(4)	4(1)	1.35(19)	$E2$	$27/2^-$	$23/2^-$
15497(2)	1694(1)	26(2)	1.38(8)	$E2$	$31/2^-$	$27/2^-$
17584(3)	2087(2)	25(2)	1.25(7)[a]	$E2$	$35/2^-$	$31/2^-$
20092(4)	2508(3)	21(2)	1.37(7)[a]	$E2$	$39/2^-$	$35/2^-$
23065(5)	2973(3)	16(2)	1.28(12)[a]	$E2$	$43/2^-$	$39/2^-$
26442(7)	3377(4)	6(1)	1.68(21)	$E2$	$47/2^-$	$43/2^-$
SD2						
13205(3)	1386(1)	4(1)	—	$(E2)$	25/2	(21/2)
	3349(3)	4(1)	0.90(12)	$\Delta I = 1$	25/2	$23/2^-$
14951(4)	1746(2)	10(1)	1.27(9)[a]	$E2$	29/2	25/2
17071(4)	2120(2)	10(1)	1.69(23)	$E2$	33/2	29/2
19571(5)	2500(3)	9(1)	1.37(7)[a]	$E2$	37/2	33/2
22530(7)	2959(4)	6(1)	1.28(12)[a]	$E2$	41/2	37/2
25769(8)	3239(4)	2(1)	1.21(16)	$E2$	45/2	41/2

[a] Doublet structure.

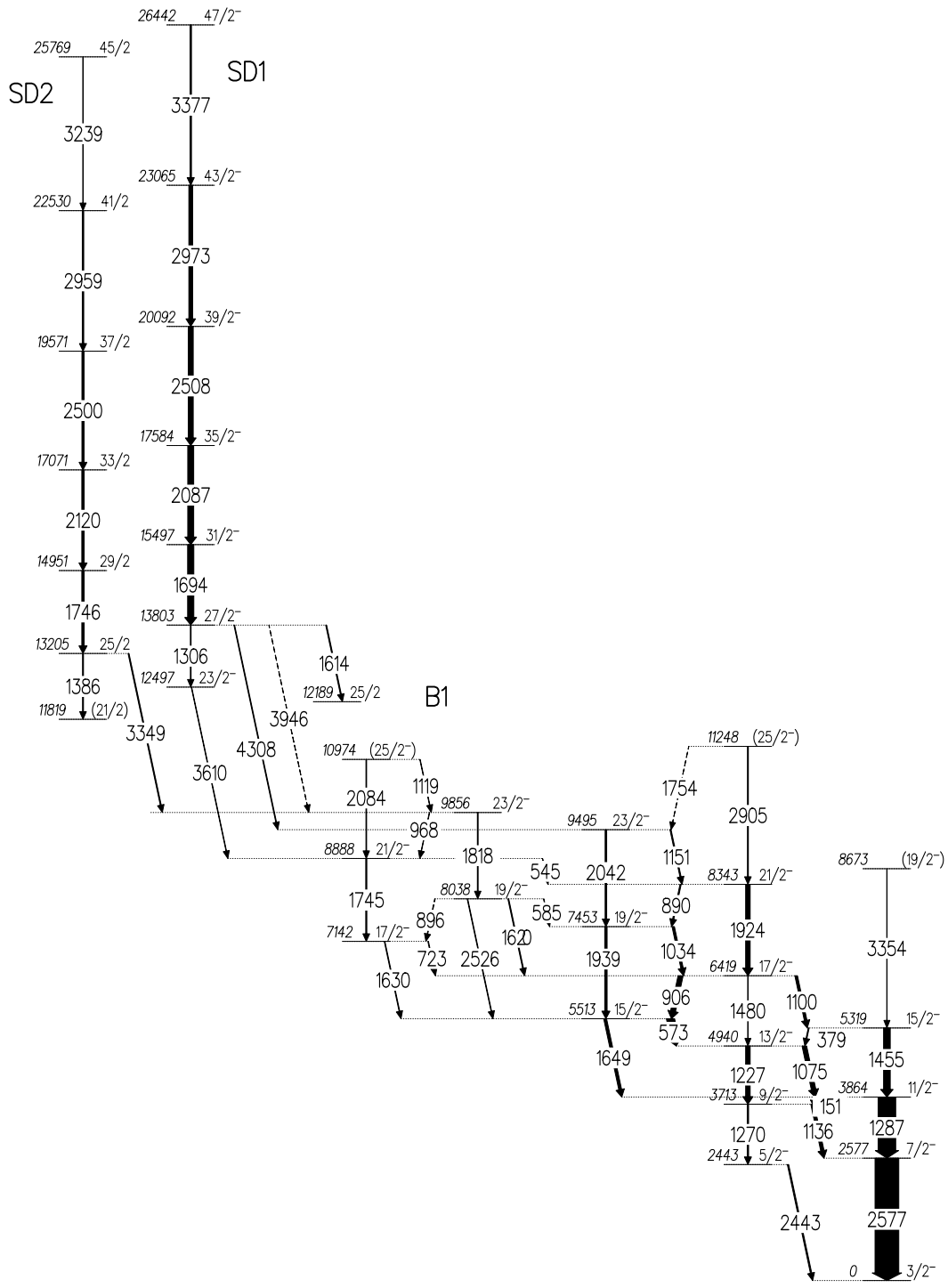

Figure 1. Relevant part of the decay scheme of ^{57}Ni. Energy labels are in keV. The widths of the arrows correspond to the relative intensities of the γ rays.

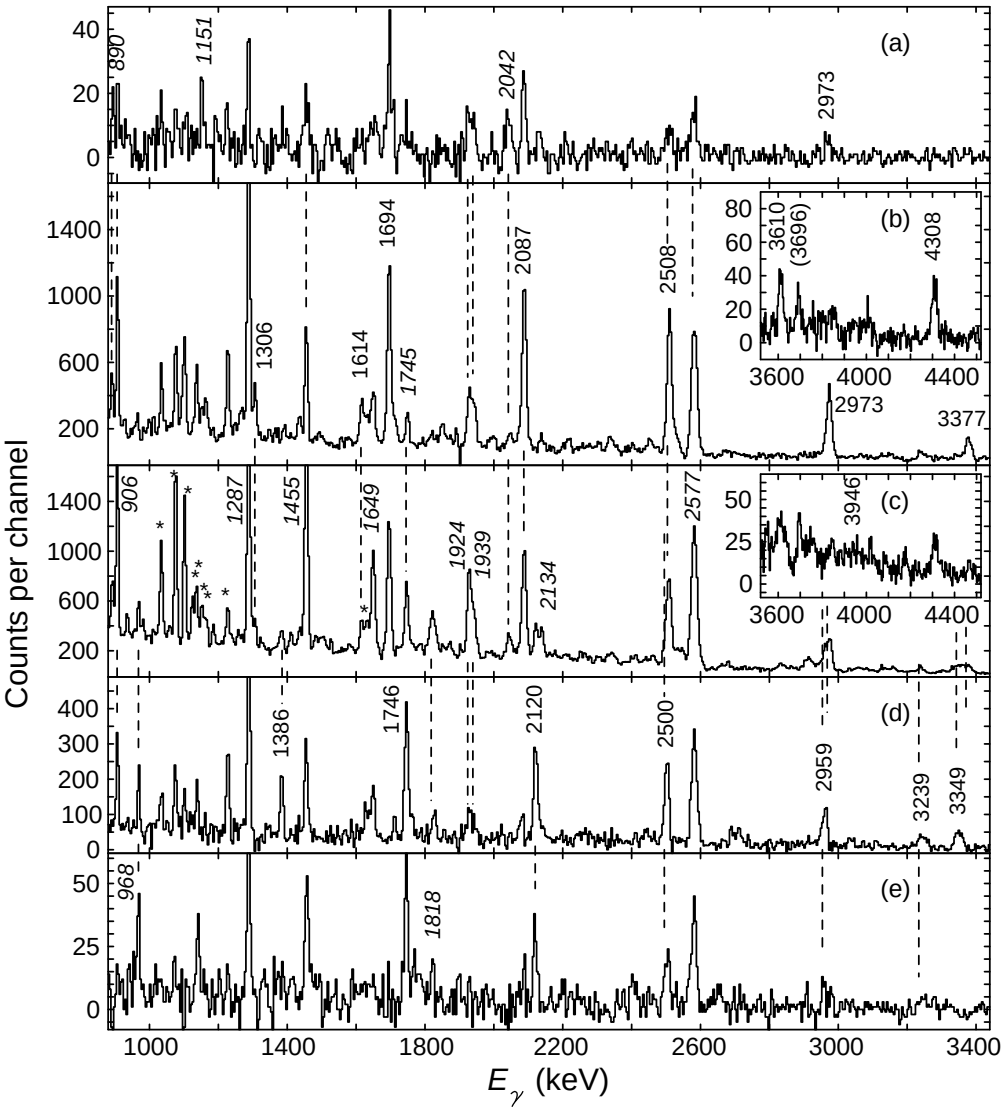

Figure 2. Reaction-channel selected γ-ray coincidence spectra representative for the newly observed rotational bands in ^{57}Ni. All spectra are in prompt coincidence with two protons and one neutron detected following ^{32}S+^{28}Si fusion-evaporation reactions. A total-energy and γ-ray fold selection method [33] has been applied to select γ-rays originating from ^{57}Ni residues. Panel (a) is taken in coincidence with the 4308 keV linking transition of band SD1. Panel (b) is the sum of spectra in coincidence with the SD1 transitions at 1694, 2087, 2508, 2973, and 3377 keV. Panel (c) is the sum of spectra of the two most intense transitions in ^{57}Ni at 1287 and 2577 keV. Panel (d) is the sum of spectra in coincidence with the 1746, 2120, 2500, 2959, and 3239 keV transitions placed in band SD2. Panel (e) is taken in coincidence with the 3349 keV linking transition of SD2. The binning is 4 keV per channel. Peak labels are energies in keV. The labels are slanted in case the corresponding peak relates to a transitions located in the spherical part of the level scheme, likewise the peaks marked with an asterix. The dashed vertical lines are guidelines. For more details see text.

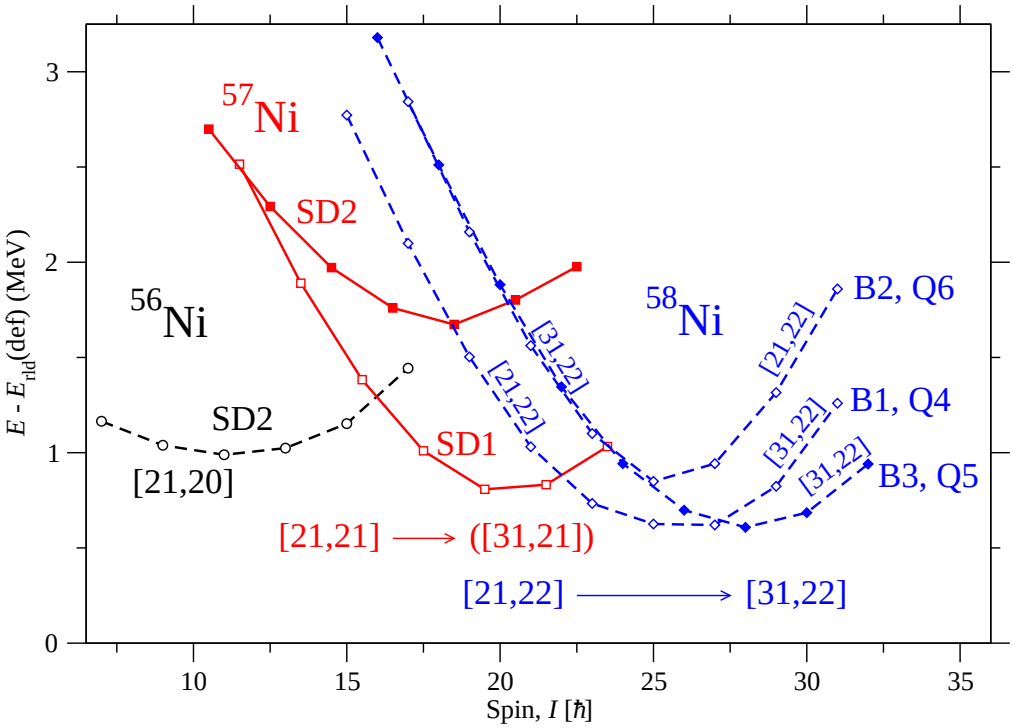

Figure 3. Observed rotational bands in ^{56}Ni [7] (dashed lines, circles), ^{57}Ni (full lines, squares), and ^{58}Ni [16] (dashed lines, diamonds), which are interpreted as having one, two, and three $1g_{9/2}$ particles, respectively. They are plotted relative to the rotating liquid drop energy, E_{rld}, as a function of spin. The ^{58}Ni bands are labelled B1, B2 and B3 in [16] and Q4, Q5 and Q6 in [17], and with standard CNS labels (see text) at low and high spin. The arrows indicate that the configuration of the yrast ^{58}Ni band has two $1f_{7/2}$ proton holes at low spin and three such holes at high spin. A similar transition occurs for the ^{57}Ni yrast band according to the interpretation in figure 4.

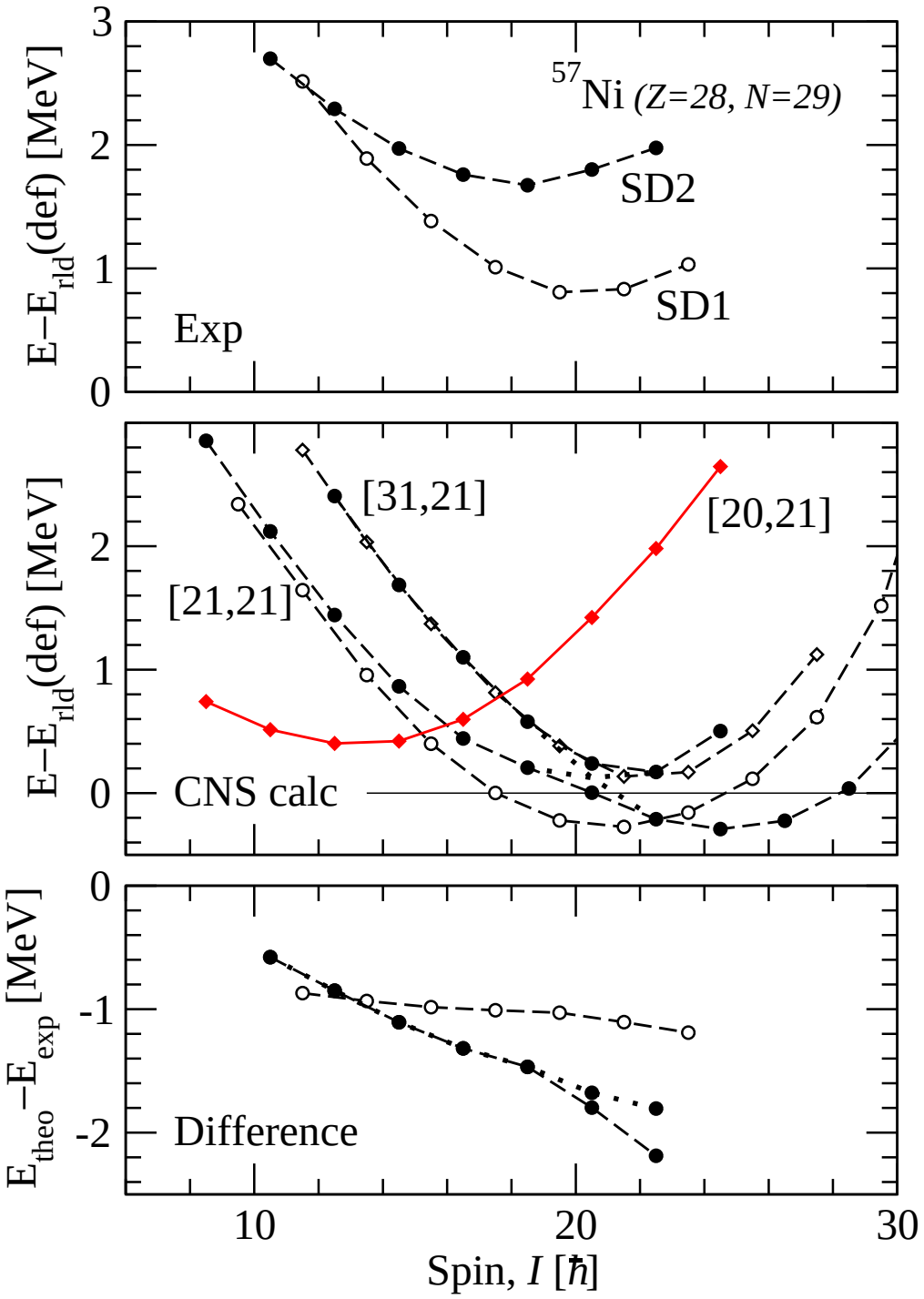

Figure 4. The upper panel shows the observed SD bands in ^{57}Ni drawn as in figure 3. The middle panel provides the calculated bands with one and two $1g_{9/2}$ particles relative to the same rotating liquid-drop reference, E_{rld}. The difference between calculations and experiment is shown in the lower panel. See text for details.

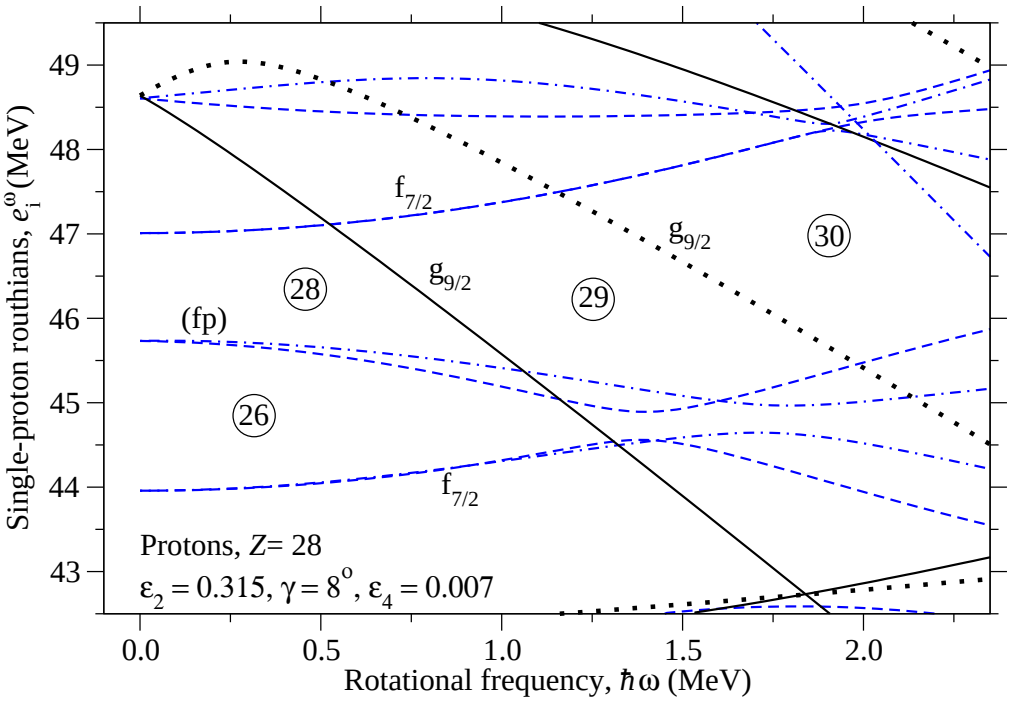

Figure 5. Proton Routhians, i.e. proton single-particle energies in the rotating frame, e_i^ω, shown as a function of rotational frequency at the approximate deformation calculated for the lowest energy $\pi(g_{9/2})^1\nu(g_{9/2})^1$, $\alpha = -1/2$ band for spin values $I = 39/2$, $43/2$, and $47/2$. In this spin range, the band interacts with the next highest band with the same symmetry (cf. figure 4), while the deformation remains essentially constant.